Carbon Dots Anchored Bacterial Cellulose Hybrid Platform as Fluorescent Sensor and Photocatalytic Remover of Pharmaceutics

Nirmiti Mate [a], Kallayi Nabeela [a], and Shaikh M. Mobin* [ab].

[a] Department of Chemistry, Indian Institute of Technology Indore, Simrol, Khandwa Road, Indore 453552, India.

[b] Centre for Advanced Electronics (CAE), Indian Institute of Technology Indore, Simrol, Khandwa Road, Indore 453552, India

*Corresponding author

Email: xray@iiti.ac.in (Shaikh M. Mobin)

Tel.: +91-731-2438752

1. Experimental Section

1.1 Characterization

The prepared samples were thoroughly characterized to functionally elucidate the structure, morphology, particle shape, size, surface area, and energy absorption sites. The structure was determined and highlighted by X-ray diffraction (XRD) analyses with Cu Kα radiation (model D/max2200PC, Rigaku Co., made in Japan). The morphology and micro-structure of samples were characterized by scanning electron microscopy (SEM) (Verios 460, FEI, USA), and transmission electron microscopy (TEM) (Tecnai G2 F20, FEI, USA). The particle shape and size were determined from TEM images, and surface electronic states were evaluated by using X-ray photoelectron microscopy (XPS) using PHI 5000 Versa Probe II (ULVAC-PHI Inc., USA) equipped with a micro-focused (200 mm, 15 kV) monochromatic Al Ka X-ray source (hn = 1486.6 eV). Photoluminescence spectra was determined using a Fluoromax-4 spectrofluorometer (HORIBA Jobin Yvon, model FM100) with an excitation and emission slit width of 2 nm in a quartz cell (1 cm × 1 cm). The Fourier transform infrared (FTIR) spectra were collected in the 4000−400 cm^{-1} range using an attenuated total reflectance-Fourier transform infrared spectroscope (ATR-FTIR) (Bruker Alpha II system). The absorption spectra in the photocatalytic degradation process were conducted by Shimadzu 2100 UV−visible spectrometer. The specific surface areas of the aerogels were measured by the Brunauer−Emmett−Teller (BET) method using Autosorb-1C (AX1C-MP-LP) at 298 K. The pore size distribution was obtained by the Barrett−Joyner−Halenda (BJH) method. Electrospray Ionization Quadrupole time-of-flight Liquid Chromatography-Mass Spectrometer (LC-MS) designed by a Bruker MicrOTOF-Q II Daltonik utilized for exact mass and true isotopic measurements.

1.2 Quantum yield (QY)

The QY of M-CDs was determined by using quinine sulfate as the reference standard solution. It was calculated using the following equation;

$$\Phi = \Phi_{QS} \times \frac{S_S}{S_{QS}} \times \frac{A_S}{A_{QS}} \times \frac{n_s 2}{n_{QS} 2} \quad (1)$$

Whereas, Φ and Φ_{QS} are the QYs of the M-CDs and quinine sulfate, respectively. A_S and A_{QS} represent the absorbance, S_S and S_{QS} are integrated intensity and n_S and n_{QS} represent the refractive indices of M-CDs and quinine sulfate, respectively.

1.3 Detection of TET and DOX with M-CDs

For analyzing the selectivity of synthesized M-CDs towards pharmaceuticals, different antibiotics *viz.* TET, DOX, NOR, AMP, VAN, CIP, ERY, and STR were checked. The interactions between M-CDs and various analytes were analyzed using FL studies, where the concentration of M-CDs was set as 11.2 mg mL^{-1}, mixed with 200 μM of different antibiotics. The solution was kept in static condition to maintain the equilibrium for 1 min. Each of the samples was studied at least three times. The FL spectra of the resulting solutions were recorded under the same experimental conditions.

Further, sensitivity studies were carried out with TET and DOX. A series of TET and DOX and M-CDs (11.2 mg mL^{-1}) with different concentrations of TET and DOX (0-200 μM) were prepared and their FL signals were recorded. Afterward, to explore the selectivity of M-CDs for TET and DOX detection while coexisting with other antibiotics such as NOR, AMP, VAN, CIP, AMO, and STR were also checked by FL spectroscopy.

The limit of detection (LOD) was calculated by the following equation:

$$LOD = 3.3\,\sigma/S \qquad (2)$$

Where σ is the error and S is the slope of the calibration plot.

The Stern-Volmer equation was used to determine the quenching constant (K_{sv}):

$$\frac{I_0}{I} = 1 + K_{sv}[C] \qquad (3)$$

where I_0 and I are the CDs' emission intensities before and following the addition of analytes, respectively, and [C] is the analyte concentration. All the experiments were triplicated under similar conditions.

The stability tests of M-CDs under different conditions such as ionic strength, pH, and temperature are performed with the aid of FL spectroscopy.

1.4 Antibiotics detection in real samples

The reliability of this analytical sensor for real-time applications was checked using milk (procured from a local milk shop), tap water (from the laboratory), groundwater (Simrol, Indore), and seawater (Arabian Sea, Mumbai). The milk samples for detecting TET and DOX were prepared using the previously reported literature.[1] Briefly, the raw milk was diluted 2.5

times then the pH of milk was lowered to 4.5 by adding 10 % trifluoroacetic acid. Then sonicate the above solution at room temperature for 15 min. This solution was centrifuged for 15 min at 12000 rpm to get a clear supernatant, which was again neutralized via 30 % NaOH and again centrifuged to remove any deposit. Further, water samples and milk samples were spiked with different concentrations of TET and DOX, separately and sensing of the same was performed.

1.5 M-CDs@BC sensing TET and DOX

FL detection tests of various antibiotics by M-CDs@BC were carried out with a similar procedure adopted for M-CDs. The M-CD@BC hydrogel (3×3×0.5 cm^3 hydrogel) was immersed in different antibiotics such as TET, DOX, NOR, AMP, VAN, CIP, ERY, and STR prepared in 50 mL (200 μM) and further incubated for 5 min prior FL analysis. The FL sensitivity of M-CD@BC towards TET and DOX was also examined by analyzing different concentrations of analyte (ranging from 0-200 μM).

1.6 Photocatalytic experiments

The photocatalytic studies of as-synthesized M-CDs were performed towards the degradation of TET and DOX aqueous solution under sunlight irradiation. Two 50 mL experimental solution mixtures were prepared each containing M-CDs (11.2 mg/mL) spiked with TET and DOX (20 mg L^{-1}) separately. The mixtures were allowed to achieve adsorption and desorption equilibrium in the dark under continuous stirring for approximately 15 min. Afterward, all the photocatalysis experiments were performed under natural sunlight (from 11:30 am to 1:30 pm on March 2023 at IIT Indore campus, Simrol, India, with an average sunlight intensity of 1 kW/m^2). At an interval of 15 min, 3 mL of solution was collected and the changes in concentrations of TET and DOX were measured by noting λ_{max} in UV-vis spectrophotometer. The photodegradation of TET and DOX antibiotics was calculated using Eq. 4

$$\%\ Degradation = \frac{(C_0 - C_t)}{C_0} \times 100 \quad (4)$$

Where, C_0 and C_t are the initial and remaining concentration at time t, respectively for TET and DOX.

Additionally, the values for photocatalytic degradation of TET and DOX were fitted to a pseudo-first-order equation (Eq. 5) and the rate constant (k) was calculated from the corresponding slope of a fitting line.

$$-ln(C_t \mid C_0) = kt \qquad (5)$$

The further photocatalytic performance of M-CDs@BC hydrogel (3×3×0.5 cm^3) towards the degradation of TET and DOX under sunlight was investigated. Briefly, the hydrogel containing TET and DOX solutions were separately stirred under dark for 15 min to ensure the achievement of adsorption-desorption equilibrium. After that the above mixture was exposed to solar light to initiate photodegradation and an aliquot solution of 3 mL was taken every 15 min degradation of TET and DOX was determined using UV-visible spectroscopy. The % degradation and the rate of reaction were determined by using Eq. 4 and 5, respectively. After each cycle, the M-CDs@BC were washed thoroughly with dilute acid and multiple times with DI and resuspended into fresh TET and DOX for 5 cycles. All the experiments for TET and DOX were conducted separately.

1.7 Electrochemical photocurrent measurement

The photocurrent using the amperometry i–t curve mode and electrochemical impedance spectra (EIS) over a frequency range of 1 to 105 Hz with an AC voltage amplitude of 10 mV were recorded in AUTOLAB PGSTAT 204N electrochemical workstation and all the electrochemical measurements were carried out using three-electrode cell with 0.5 M Na_2SO_4 as an electrolyte. The M-CDs sample as a working electrode, Ag/AgCl as a reference, and Pt wire as a counter electrode were utilized. All the photo-electrochemical measurements were conducted using a blue light source with 100 mW cm^{-2} power density.

2. XPS deconvoluted spectra of M-CDs

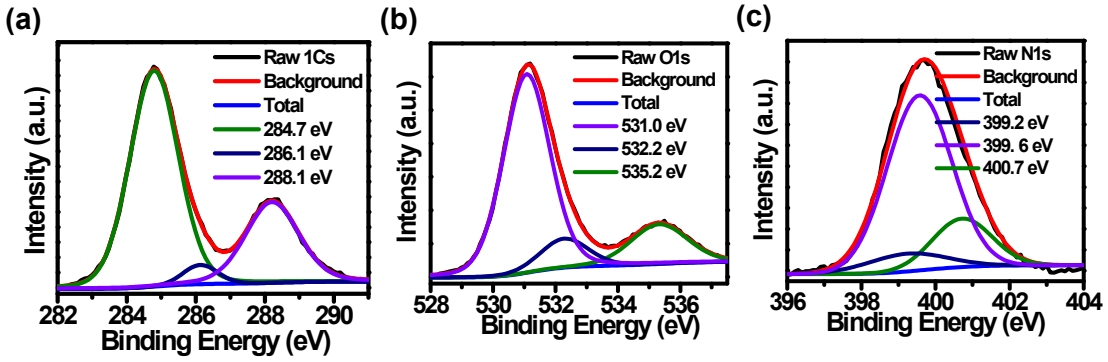

Figure S1. High-resolution XPS spectra of M-CDs (a) C1s (b) O1s (c) N1s.

3. Stability test of M-CDs under various conditions

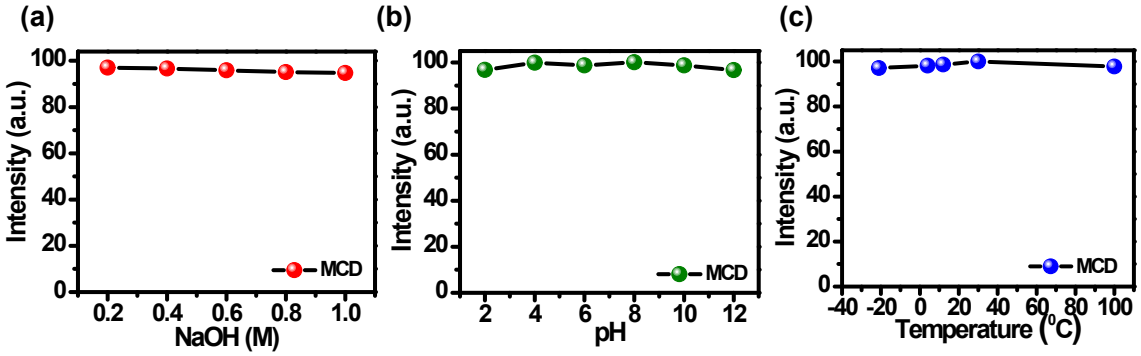

Figure S2. Stability plot of M-CDs in the presence of (a) NaOH (b) pH and (c) temperature.

4. SEM image of BC

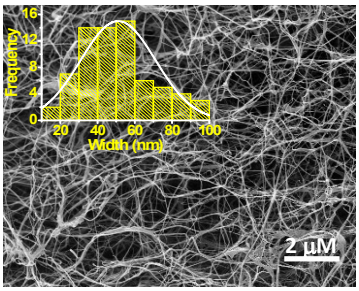

Figure S3. BC showing nanofibrous porous network structure (inset: histogram from a width of cellulose fibers).

5. BET-BJH analysis

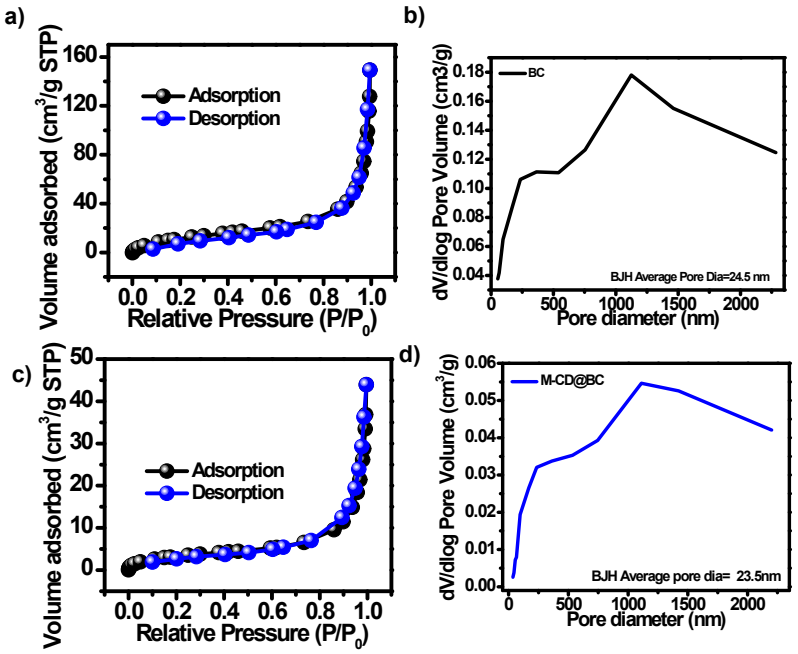

Figure S4. Nitrogen adsorption and desorption analysis conducted for control pristine BC and M-CD@BC aerogels: a) BET adsorption isotherms and b) corresponding BJH pore volume plots for BC. c) BET adsorption isotherms d) corresponding BJH pore volume plots for M-CD@BC.

6. Comparative XPS Spectrum of M-CD, BC and M-CD@BC

The XPS survey scan recorded for M-CD@BC, BC, and M-CDs are compared in Figure S4. The XPS of M-CDs reveals the presence of carbon (C), oxygen (O), and nitrogen (N) (Red line) and survey scan spectra of BC exhibited two peaks at 284.0 and 530.4 eV, indicative of presence of C and O, respectively (Figure S5; grey line). Further, the survey spectrum of M-CD@BC proves the coexistence of C, N, and O elements (Figure S5 ; blue line), which confirm the anchoring of M-CDs on BC due to reoccurrence of N peak in M-CD@BC. These observations signify the successful incorporation of M-CDs onto BC.

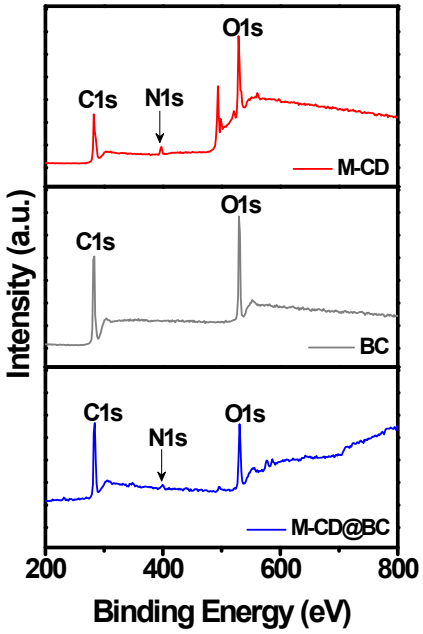

Figure S5. Comparative XPS survey spectra of M-CD, BC and M-CD@BC.

7. UV-vis spectra of BC and M-CD@BC

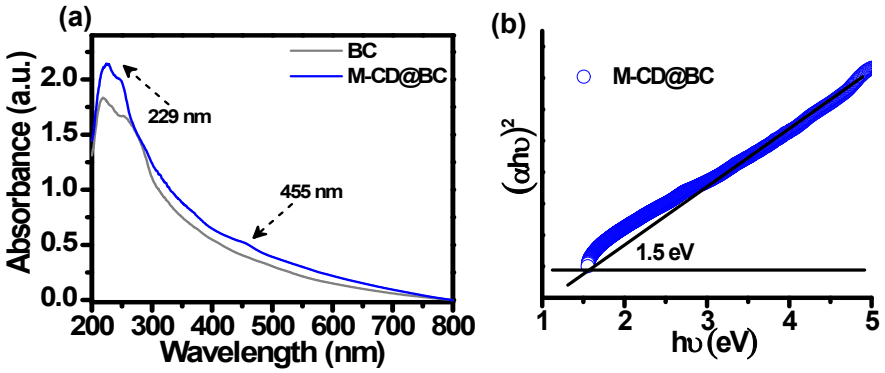

Figure S6. (a) Absorbance spectra of BC (grey line) and M-CD@BC (blue line), (b) band gap estimation of M-CD@BC.

8. M-CD@BC images under visible and UV illimitation (l_{ex}=365 nm)

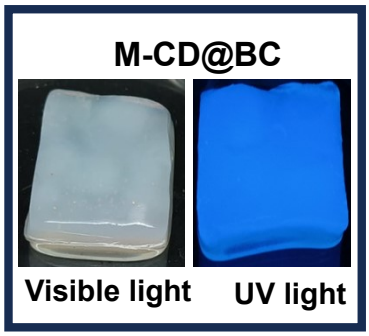

Figure S7. The vertical view photograph of M-CD@BC under (a) visible, and (b) UV light (365 nm).

9. Linearity Plot

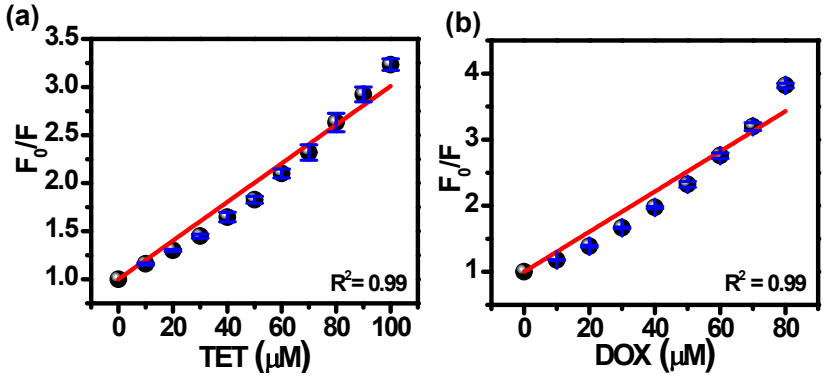

Figure S8. The linearity plot of F/F_0 vs different concentrations of (a) TET and (b) DOX.

10. Interference studies in the presence of various antibiotics

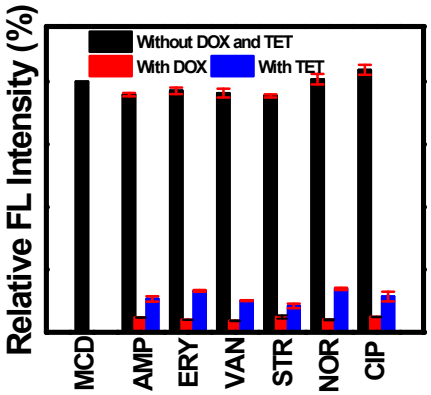

Figure S9. Competitive selectivity in the sensing response of M-CDs in the presence of various antibiotics compounds ($c = 1.0 \times 10^{-2}$ M).

11. Mechanism of sensing

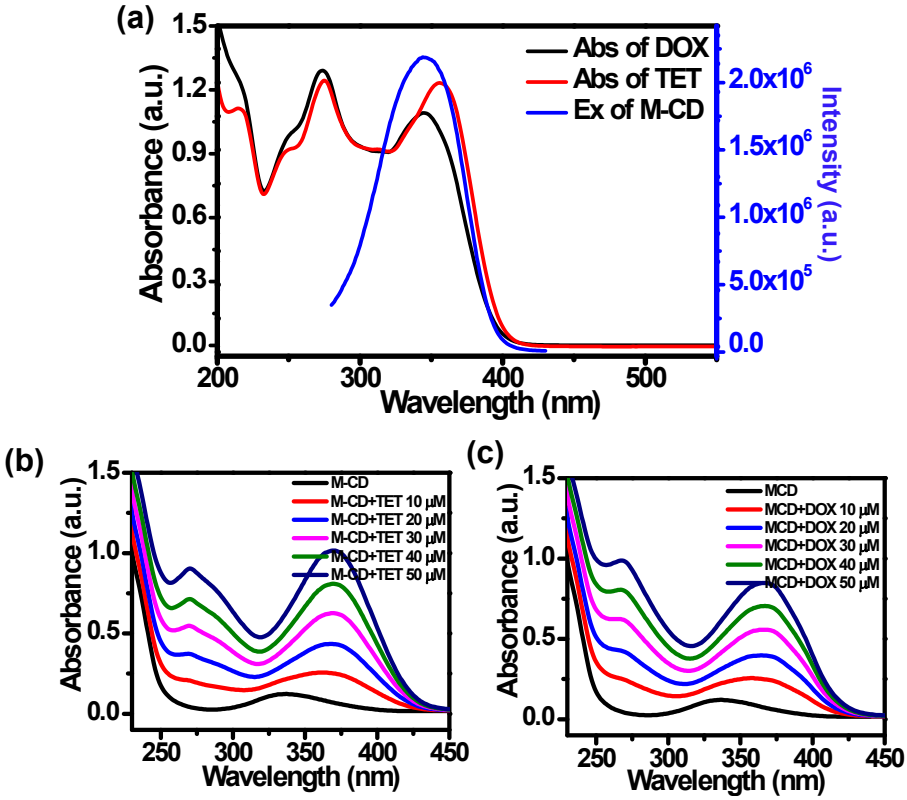

Figure S10. a) UV-vis absorption spectra of TET and DOX showing spectral overlapp with with fluorescence excitation of M-CDs. UV–vis spectra of M-CD for different concentration of b) TET and c) DOX.

12. Sensing studies of TET and DOX with M-CD@BC

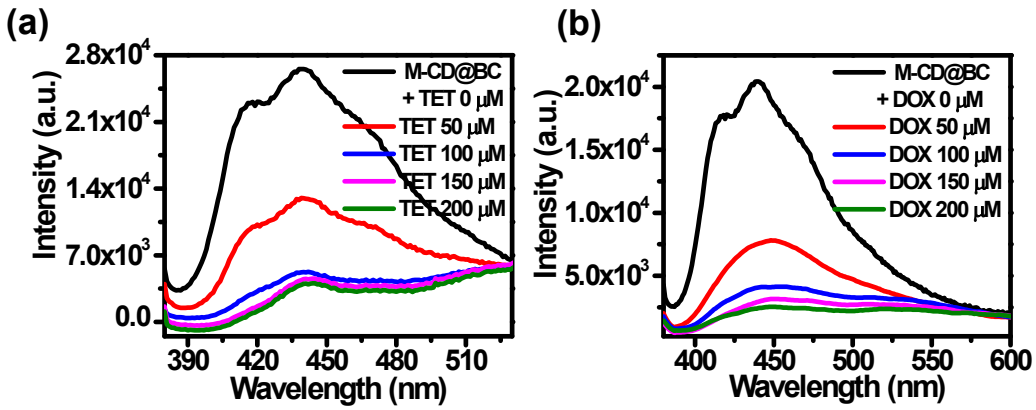

Figure S11. Fluorescence response of M-CD@BC in the presence of an increasing concentration of (a) TET and (b) DOX (from 0-200 μM).

13. Interference study with M-CD@BC

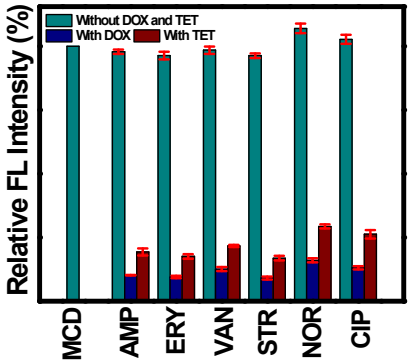

Figure S12. Interfering studies for sensing response of M-CD@BC in the presence of various antibiotics (c = 1.0 × 10^{-2} M).

14. Reusability of M-CD@BC for detection of TET and DOX

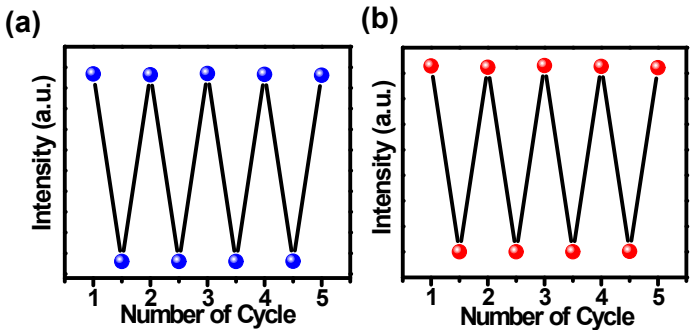

Figure 13. Recyclability study for M-CD@BC (a) TET and (b) DOX (200 μM).

15. Degradation studies under different antibiotic concentrations

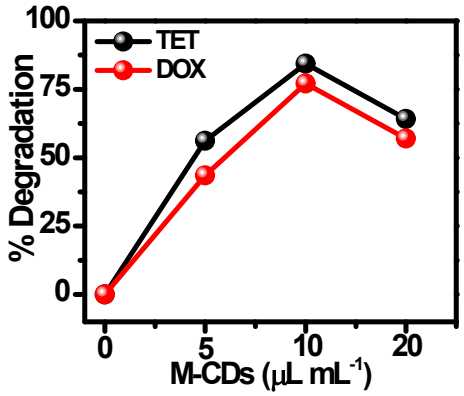

Figure S14. Photocatalytic degradation studies of TET and DOX under various concentration of M-CDs.

16. Comparative % Degradation of TET and DOX

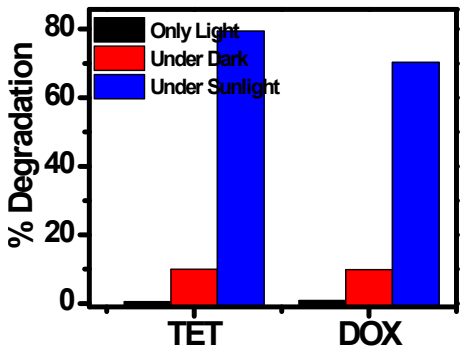

Figure S15. The degradation percentage of TET and DOX under sunlight without M-CDs, in the dark, and in sunlight with catalyst M-CDs

Table S1: Comparison of photocatalytic degradation of antibiotics tetracycline (TET) and doxycycline (DOX) by various photocatalysts.

Sr. No.	Catalyst	Pollutant	Concentration (ppm)	Time (Mins)	% Degradation	Light Intensity	Reference
1.	N-CQDs/BiPO4	TC	20	150	70	UV light source	2
2.	GQDs/mpg-C_3N_4	TC	20	120	67	300 W Xe arc lamp ($\lambda > 400$ nm)	3
3.	$BiVO_4$/N-CQDs/Ag_3PO_4	TC	10	90	59.8	A 300 W Xe lamp (320 nm<k <780 nm, light intensity: 160mW/cm^2)	4
4.	GQDs/g-CNNR	TC	15	120	80	300 W xenon lamp (420 nm cutoff filter)	5
5.	CQDs/ $PbBiO_2Cl$	TC	20	120	74.3	300 W Xe-lamp (400 nm light-cut filter)	6
6.	$LaFeO_3/SnS_2$	TC	20	120	28.8	300 W, Xe lamp	7
7.	$CuBi_2O_4$/BiOBr	TC	20	150	64.7	300 W, Xe lamp	8

8.	Vis/CDs-ZIS/PS	TC	20	120	83	Visible Light	9
9.	M-CDs	TET & DOX	20	120	79.4 and 70.3	Sunlight	This Work
10.	M-CD@BC	TET & DOX	20	120	74.2 and 64.0	Sunlight	This Work

17. Electrochemical studies

The transient photocurrent response of M-CDs and the bare electrode was obtained for several on-off cycles under visible light exposure and depicted in Figure S16a. The response of M-CDs to visible light on-off cycle is significantly stronger compared to the bare sample. This is due to the excellent separation of photogenerated electrons and holes in M-CDs, which reduces the recombination of photogenerated carriers. The enhanced photogeneration of charge carriers could result in increased photocatalytic activity of M-CDs. The EIS was conducted to further evaluate the charge transfer and recombination mechanism. Figure S16b demonstrates that the arc radius on the EIS Nyquist plot of M-CDs appears smaller than that of the bare sample when examined under visible light illumination. This suggests that there is an efficient separation of photogenerated electron-hole pairs and a more rapid charge transfer. This would enhance the photocatalytic activity.

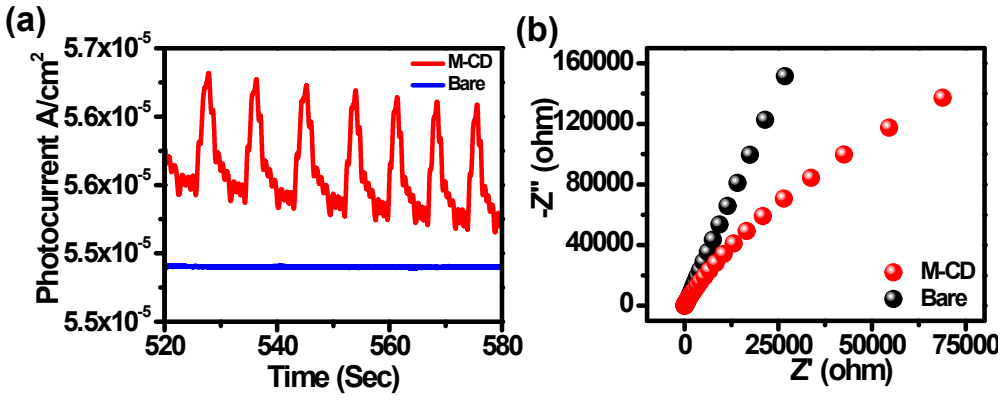

Figure S16. (a) Transient photocurrent density versus time plotted, and (b) EIS Nyquist plots of M-CDs under visible light in 0.5 M Na_2SO_4 electrolyte.

18. Removal of antibiotics studies

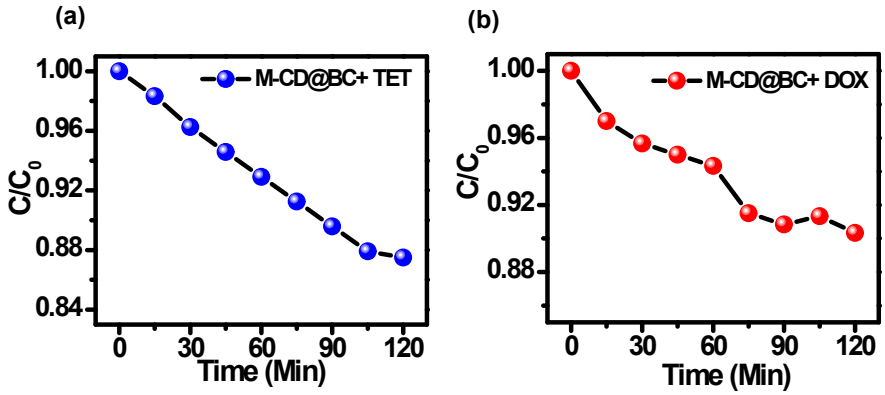

Figure S17. Removal of (a) TET, and (b) by M-CD@BC without sunlight illumination (experimental conditions: C_0 = 20 mg L−1).

19. Kinetics of M-CD@BC towards TET and DOX

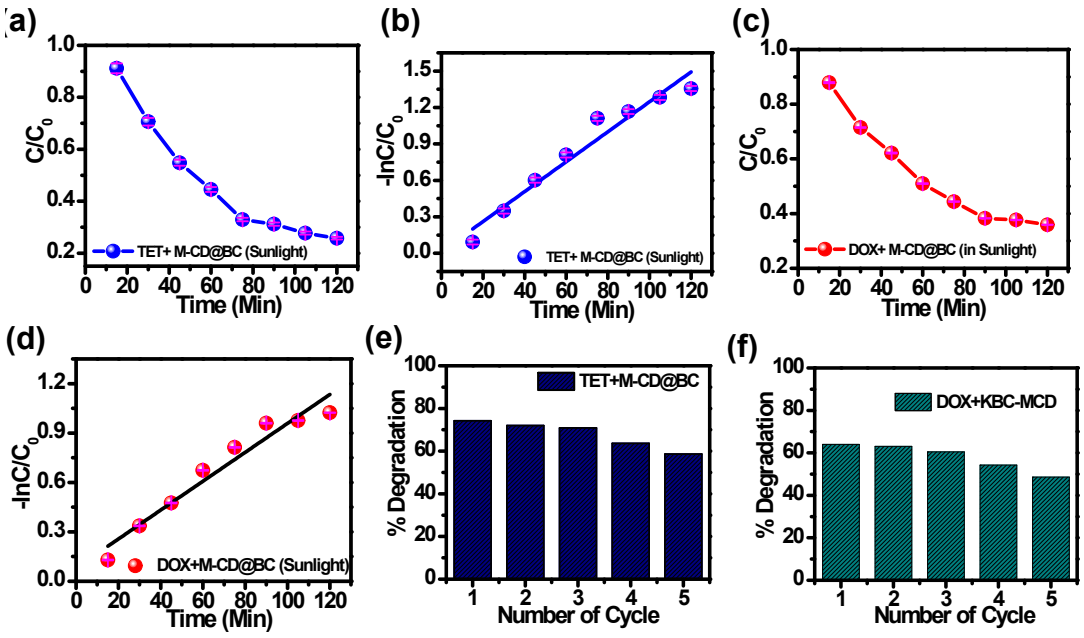

Figure S18. a, b) Photodegradation of TET under sunlight and their rate, respectively, c, d) photodegradation of DOX under sunlight and their rate, respectively. Recyclability study of composite hydrogel M-CD@BC towards e) TET and f) DOX.

20. Degradation pathway of TET and DOX analysed by mass spectra

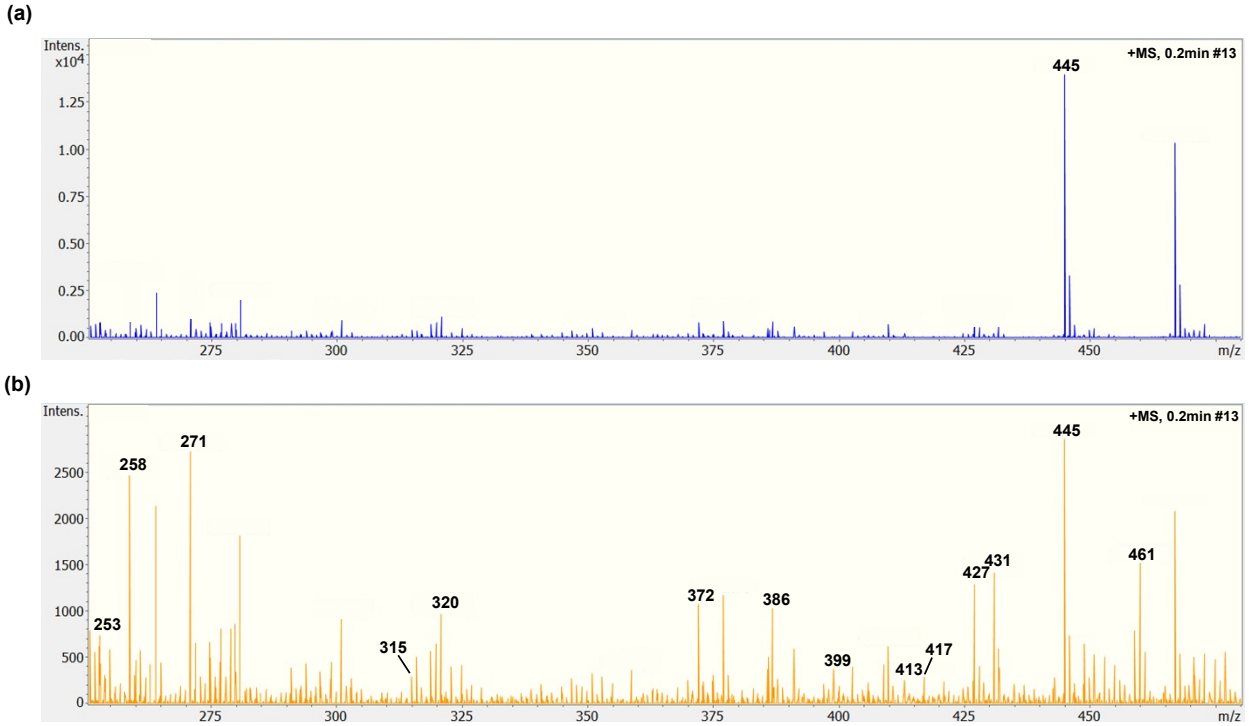

Figure S19. Mass spectra of (a) initial TET solution at 0 min, (b) degradation of TET in 120 min and intermediate detected.

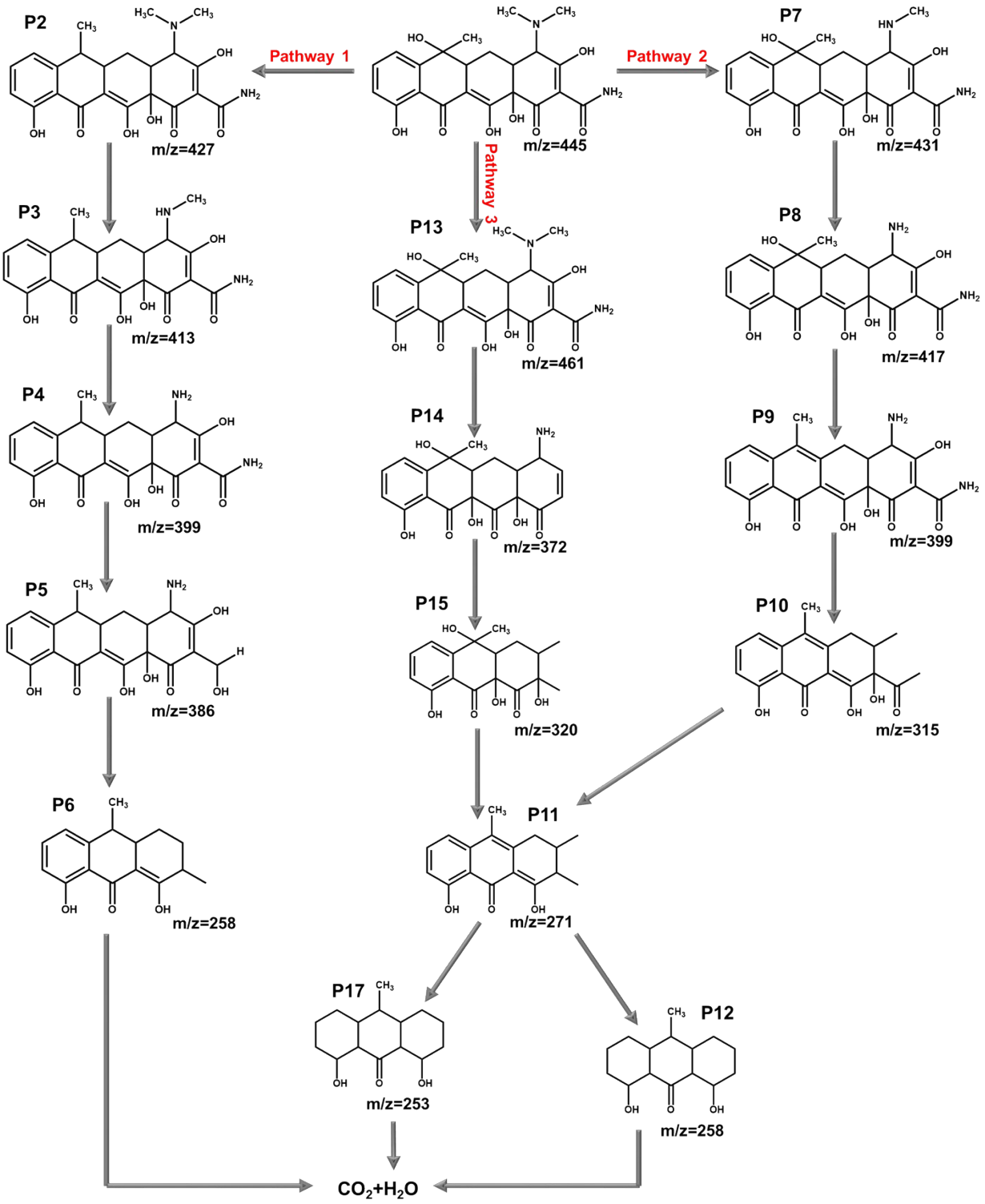

Scheme S1. Suggested pathway for photocatalytic degradation of TET and their intermediates.

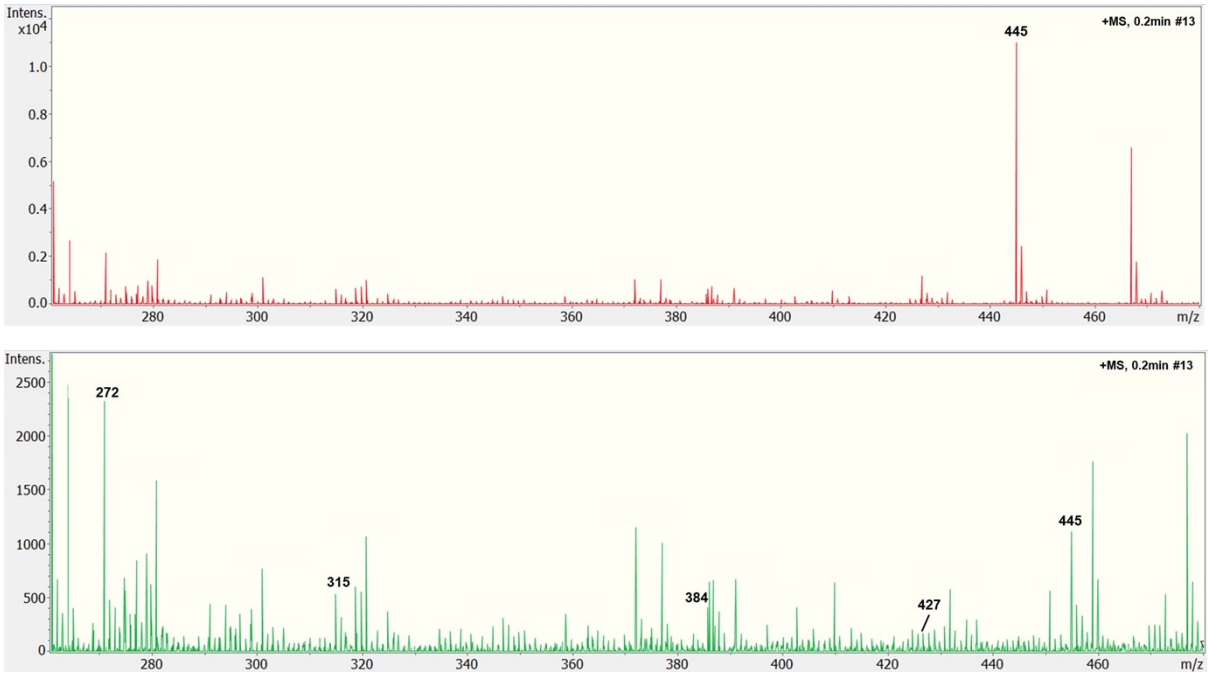

Figure S20. Mass spectra of (a) initial DOX solution at 0 min, (b) degradation of DOX in 120 min and intermediate detected.

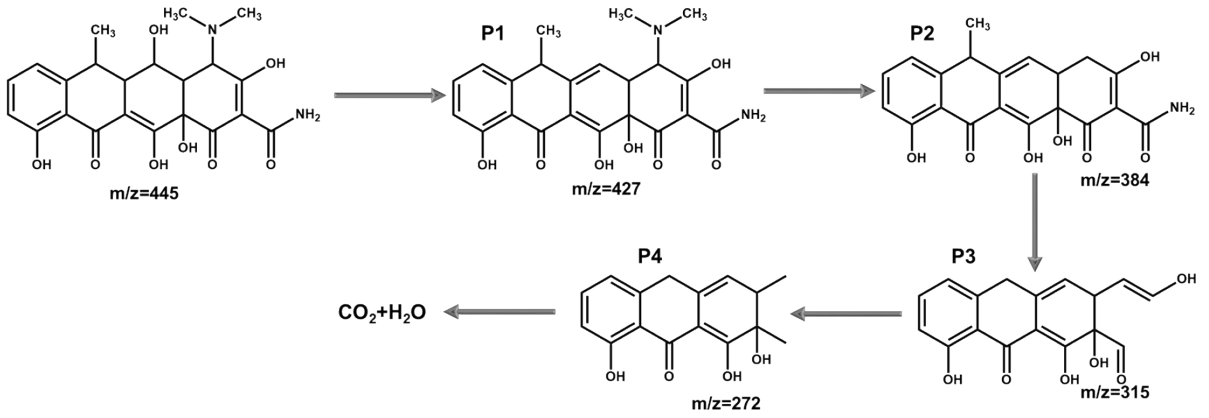

Scheme S2. Suggested pathway for photocatalytic degradation of DOX and their intermediates.

References

1 N. Kaur, P. Tiwari, Z. Abbas and S. M. Mobin, *J. Mater. Chem. B*, 2022, **10**, 5251–5262.

2 J. Di, J. Xia, X. Chen, M. Ji, S. Yin, Q. Zhang and H. Li, *Carbon*, 2017, **114**, 601–607.

3 J. Liu, H. Xu, Y. Xu, Y. Song, J. Lian, Y. Zhao, L. Wang, L. Huang, H. Ji and H. Li, *Applied Catalysis B: Environmental*, 2017, **207**, 429–437.

4 J. Zhang, M. Yan, X. Yuan, M. Si, L. Jiang, Z. Wu, H. Wang and G. Zeng, *Journal of Colloid and Interface Science*, 2018, **529**, 11–22.

5 A. Yuan, H. Lei, F. Xi, J. Liu, L. Qin, Z. Chen and X. Dong, *Journal of Colloid and Interface Science*, 2019, **548**, 56–65.

6 Y. Sheng, D. Yi, H. Qingsong, W. Ting, L. Ming, C. Yong, S. Yifan, D. Jun, W. Bin, J. Xia and L. Huaming, *Journal of Photochemistry and Photobiology A: Chemistry*, 2019, **382**, 111921.

7 J. Luo, R. Li, Y. Chen, X. Zhou, X. Ning, L. Zhan, L. Ma, X. Xu, L. Xu and L. Zhang, *Separation and Purification Technology*, 2019, **210**, 417–430.

8 S. Huang, G. Wang, J. Liu, C. Du and Y. Su, *ChemCatChem*, 2020, **12**, 4431–4445.

9 W. Shi, C. Hao, Y. Fu, F. Guo, Y. Tang and X. Yan, *Chemical Engineering Journal*, 2022, **433**, 133741.